Scientific Research Publishing

World Journal of Condensed Matter Physics, 2024, 14, 77-95
https://www.scirp.org/journal/wjcmp
ISSN Online: 2160-6927
ISSN Print: 2160-6919

Hexagon-Islands Density and Size Distribution on Growing Single-Walled Carbon Nanotubes in the Kinetic 5-Vertex Model

Sènan Ida Valérie Hontinfinde[1*], Josaphat Adda[1], Joel Kple[2,3], Franck Zounmenou[2], Félix Hontinfinde[2,3]

[1]ENSGMM, Université d'Abomey (UNSTIM), Abomey, Bénin
[2]Département de Physique, Université d'Abomey-Calavi, Abomey-Calavi, Benin
[3]IMSP, Université d'Abomey-Calavi (UAC), Dangbo, Bénin
Email: *vhontinfinde26@gmail.com

How to cite this paper: Hontinfinde, S.I.V., Adda, J., Kple, J., Zounmenou, F. and Hontinfinde, F. (2024) Hexagon-Islands Density and Size Distribution on Growing Single-Walled Carbon Nanotubes in the Kinetic 5-Vertex Model. *World Journal of Condensed Matter Physics*, **14**, 77-95.
https://doi.org/10.4236/wjcmp.2024.144008

Received: October 1, 2024
Accepted: November 23, 2024
Published: November 26, 2024

Abstract

A kinetic 5-vertex model is used to investigate hexagon-islands formation on growing single-walled carbon nanotubes (SWCNT). In the model, carbon atoms adsorption and migration processes on the SWCNT edge are considered. These two dynamic processes are assumed to be mutually independent as well as mutually dependent as far as the whole growth of the nanotube is concerned. Key physical parameters of the model are the growth time t, the diffusion length Γ defined as the ratio of the diffusion rate D to the carbon atomic flux F and the SWCNT chiral angle. The kinetic equation that describes the nanotube edge dynamics is solved using kinetic Monte Carlo simulations with the Bortz, Kalos and Lebowitz update algorithm. The behaviors of islands density and size distribution are investigated within the growth parameters' space. Our study revealed key mechanisms that enable the formation of a new ring of hexagons at the SWCNT edge. The growth occurs either by pre-existing steps propagation or by hexagon-islands growth and coalescence on terraces located between dislocation steps, depending on values of model parameters. This should offer a road map for edge design in nanotubes production. We also found that in appropriate growth conditions, the islands density follows Gaussian and generalized Wigner distributions whereas their size distribution at a given growth time shows a decreasing exponential trend.

Keywords

Kinetic 5-Vertex Model, Single-Walled Carbon Nanotube, Monte Carlo Simulations, Island Density and Size Distribution, Gaussian and Wigner Distributions

1. Introduction

Materials may grow via the physical ejection of atoms or molecules onto their surfaces. The adsorbed species condense or nucleate on the substrates to form islands that can grow or coalesce to form new surface layers. This ejection technique has been widely used in several crystal growth experiments (e.g. in Molecular Beam Epitaxy) and simulations [1]-[3]. The evolution of a crystal surface subjected to an atomic flux has been a topic that has attracted much interest from physicists in the past decades [4] [5]. Most theoretical tools used to feature this evolution phenomenon comprised rates equation theory and numerical simulations [6]-[9]. Numerical simulations also provide the possibility to feature relevant growth mechanisms that determine the growth character in view of tailoring materials or thin film properties in a wide range of synthesis parameters. Using numerical simulations by Monte Carlo method or molecular dynamics, realistic predictions are possible on adatoms and island densities as well as on island size distribution in rather complex models. Less is, however, known about these physical quantities on vicinal or stepped surfaces.

Chemical vapor deposition (CVD) experiments for carbon nanotubes (CNT) growth is a nanoscale procedure that needs efficient nanoparticles as catalysts [10]-[17]. Carbon atoms issued from the decomposition of a hydrocarbon on the catalyst maintained at high temperature adsorb on the CNT end-rim. The CNT then grows and is collected upon cooling the system to room temperature. Several theoretical growth models have been devised to investigate this phenomenon, in particular in chiral CNTs growth using models with screw dislocations [18]-[20]. Some of the models have shown, among other results, that the CNT growth speed is proportional to the nanotube chirality [18].

Due to the similarity that exists between crystal surfaces and nanotubes growth, some crystal growth concepts could be applied to CNTs in view to get more insight into CNTs formation mechanisms. In this perspective, a kinetic 5-vertex model has been recently introduced to characterize zigzag [21] and chiral nanotubes growth [22]. In this model, carbon atoms can adsorb at the nanotube end-rim and stick where they land. They can also migrate to nearby adsorption sites at the CNT edge. It has been shown in Ref. [22] that models with adsorption and migration kinetics of carbon atoms at the CNT edge are able to show the experimental result that in appropriate growth conditions, the CNT growth rate is proportional to the Burgers vector, *i.e.* to the chiral angle of the CNT. More recently, a modified version of this kinetic vertex model displayed interesting fundamental results [23]. It was shown that during the CNT growth, some specific nanofacets are formed at the CNT edge. Their density is found to display a non-trivial scaling behavior with the diffusion length Γ and the growth time t. Such a behavior has been previously observed in Ref. [6] through Monte Carlo simulations of atoms island densities in deposition processes onto crystal surfaces.

The growth mechanisms of SWCNTs are still not very well understood [12] [17] [24]-[28]. Such a situation motivates the present work, where hexagon-

islands density and size distribution at the edge of a growing SWCNT are investigated by means of the previous vertex model. This study of islands statistics, not performed in our previous works, is however essential to the knowledge of details of growth kinetics and microscopic growth mechanisms of new hexagon rings at the nanotube edge. This could give some valuable insight to experimenters in designing SWCNTs with specific edge morphologies. In the model, deposition and migration events are assumed to be Markov processes and take place according to their probabilities. We find that carbon island densities display a non-trivial behavior. Depending on values of model parameters, they follow the Gaussian or the generalized Wigner distribution. On the contrary, the hexagon-island size distribution displays an exponential decrease with the growth time t.

2. Kinetic 5-Vertex Model for SWCNTs Growth

The line representation of the 8-vertex model is depicted in **Figure 1**. In **Figure 2**, the edge of a chiral SWCNT with conventional indices (15, 2) in the dislocation theory of Ding *et al.* [18] is mapped onto the 5-vertex model. Indeed, in vertex mapping of crystal surfaces (see [29] and references therein), the topmost atoms of columns are considered and should be described by one or a group of vertices. In the case of the SWCNT edge's mapping, we actually need one or two vertices: 4, 5, 6, 73, 28. The same description may also be performed with vertices 4, 5, 6, 7, 8 by omitting vertices 2 and 3 [21]-[23]. This allows the topmost carbon atom of each column to be described by only one vertex. This consideration facilitates the computation of the exact finite-size solution of the CNT growth model by the transition matrix method where vertices number conservation is required. Thus, the evolution of a portion of the CNT edge described by 5(73)6(28)4 to 56564 due to one carbon atom deposition should be simply considered as the evolution of 57684 to 56564 where the number of vertices is conserved. Vertex energies are chosen assuming that the completely flat edge (although corrugated at the microscopic level) associated with the zigzag CNT, which is only described by vertices 5 and 6, has zero energy. All other edge excitations or deformations by deposition or diffusion processes at a given column of atoms, are assumed, regardless of the coordination number of the carbon atom at the vertex, to have the same energy ϵ. This approximation becomes a very good one at high temperatures where vertex energies are less relevant in the growth dynamics (see below). It is worth noting that this approximation generated very good results in agreement with experimental findings in Ref. [22]. Hence, vertex energies are: $\epsilon_5 = \epsilon_6 = 0$; $\epsilon_4 = \epsilon_7 = \epsilon_8 = \epsilon$.

For the exact solution of the model, vertex configurations are classified into time-conserved classes subdivided into subclasses where configurations are equivalent by translations. A class is characterized by a given chiral angle related to the quantity $c = N_7 - N_8$, where N_7 and N_8 are respectively the number of vertices of types 7 and 8 at the CNT end-rim. The zigzag edge with zero chiral angle is then associated with $c = 0$.

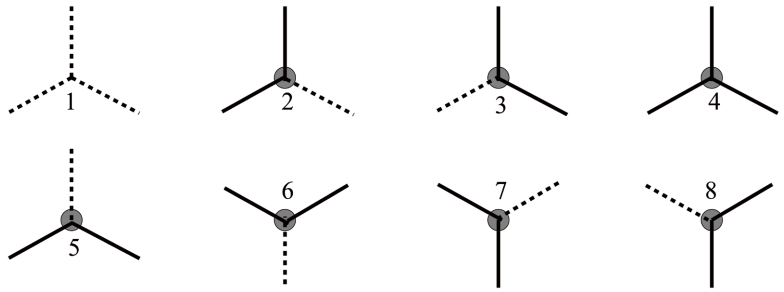

Figure 1. Schematic line representation of the 8-vertex model.

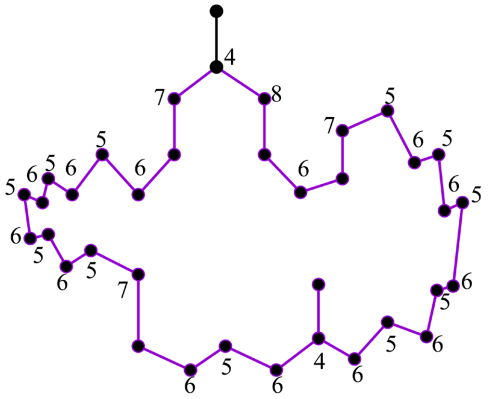

Figure 2. (color online) Mapping of a SWCNT growing edge of length $L = 30$ with conventional indices (15, 2) onto the 5-vertex model. In the description, full vertex lines are used while dashed ones are omitted [21] [22]. Vertices along the edge are labeled by moving in an anticlockwise way around the nanotube edge. Vertices 2 and 3 are omitted in the mapping (see text).

A deposition site at the CNT rim is characterized by a 5-vertex subconfiguration formed by three vertices, which we termed growth kink subconfigurations (growth active sites). Eight such kinks are found in the model:

$$K_1 = 856, \quad K_2 = 656, \quad K_3 = 857, \quad K_4 = 657,$$
$$K_5 = 464, \quad K_6 = 768, \quad K_7 = 764, \quad K_8 = 468.$$

A diffusion site at the CNT growing edge is characterized by a 5-vertex subconfiguration formed by four vertices that we termed diffusion kinks. There are also 8 different types of these kinks:

$$\bar{K}_1 = 4656, \quad \bar{K}_2 = 4657, \quad \bar{K}_3 = 4764, \quad \bar{K}_4 = 4768,$$
$$\bar{K}_5 = 6564, \quad \bar{K}_6 = 8564, \quad \bar{K}_7 = 4684, \quad \bar{K}_8 = 7684.$$

The dynamics is introduced in the model by carbon atom attachments and migrations (**Figure 3** and **Figure 4**) at the CNT edge. These events are assumed to be Markov processes. Carbon adatoms migration occurs at a hopping rate given by the conventional Arrhenius ansatz: $D = D_0 \exp(-\beta E_0)$ where D_0 denotes the attempt frequency and E_0 the hopping energy barrier, $\beta = 1/k_B T$ is the inverse synthesis temperature, k_B is the Boltzmann constant, which is set to 1 in the following.

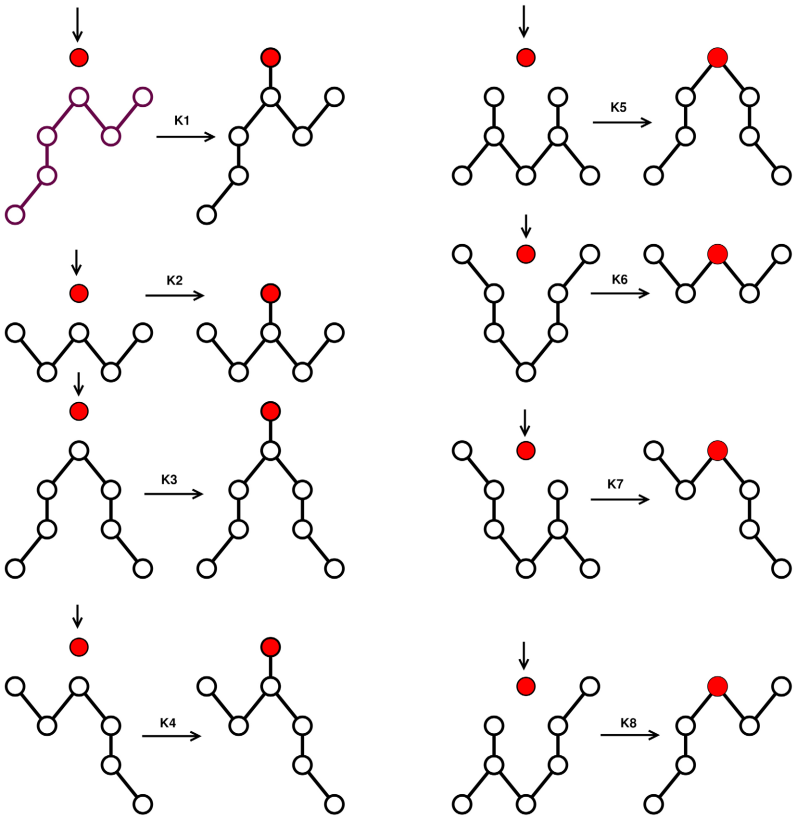

Figure 3. (color online) Schematic representations of the eight deposition events on the nanotube rim (see text) and associated rim local morphological changes.

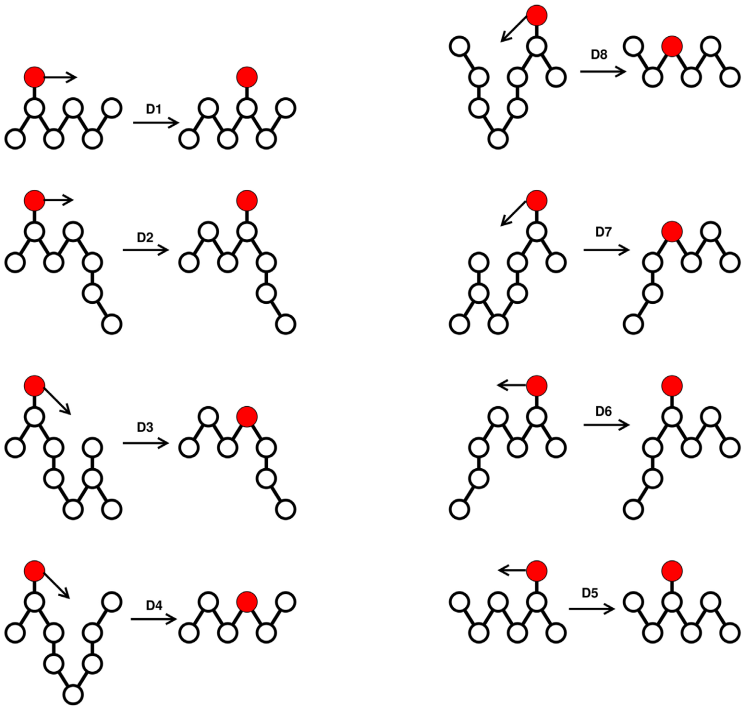

Figure 4. (color online) Schematic representations of the eight migration processes allowed on the nanotube edge (see text) and associated local morphological changes.

The constant atomic flux F is expressed in atoms per unit time. One can study its influence on the growth kinetics and the CNT edge morphology. The CNT edge relaxation occurs in the model by carbon adatoms migration processes that occur at the following rate [22]:

$$D = D_0 \frac{\exp(-\beta E_0)}{1+\exp(\beta \Delta E)}, \tag{2.1}$$

where ΔE is the change of the 5-vertex energy of the tube edge when the attempted move is realized; D_0 is the attempted frequency that is assumed to be: $D_0 \simeq kT/h$ [22] [30] where h is the Planck constant (hereafter set to 1); E_0 is the activation energy that is assumed to be a constant set to ϵ for all migration processes.

Denoting by $v = \exp(\epsilon/T)$, migration rates are summarized as follows:

$$D_1 = D_2 = D_5 = D_6 = D_0 \frac{1}{2v}, D_3 = D_7 = D_0 \frac{1}{v+v^{-1}}, D_4 = D_8 = D_0 \frac{1}{v+v^{-2}}$$

In the model, a new parameter Γ, which has the dimension of diffusion length, is defined through the relation: $\Gamma = D_1/F$. Physical quantities of interest will be evaluated as functions of the growth time t (or in the steady state) related to the number N of deposited carbon atoms, the diffusion length Γ, the synthesis temperature T, and the chiral angle of the CNT. The temperature is fixed to $T = 10$ for most islands density calculations.

3. Kinetic Monte Carlo simulations

The computational details could be found in Refs. [22] [23]. In the simulations, the two growth processes: deposition and diffusion, can be selected at a given growth time according to their probabilities, determined by means of the total evolution rate of the system. This rate is calculated assuming that all possible events at the CNT edge, are mutually independent. The kinetic Monte Carlo simulations with the Bortz, Kalos and Lebowitz (BKL) algorithm is used [31]. In the BKL scheme, a move is performed at each step according to it's *a priori* probability. For a CNT edge 5-vertex configuration (V) obtained at a given stage of the growth with Ω possible processes with transition rates $T_n, n = 1,\Omega$, the total evolution rate R of (V) is the sum of transition rates of all updated events on (V). The real life-time of (V) is given by:

$$\tau = -\log(\bar{r})/R \tag{3.1}$$

where $\bar{r}$ is a random number generated between 0 and 1. The BKL algorithm follows. A random number r_1 is selected, and a random rate $Q = r_1 \times R$ is calculated. By summing the rates of updated processes of configuration (V), the first process such that the condition

$$\sum_{n=1} T_n \geq Q \tag{3.2}$$

holds is realized. Then possible processes are updated, and the system evolution rate recalculated. After a sufficient simulation time period t where g new 5-

vertex configurations are generated, the values of physical quantities are estimated by a time-averaging procedure. The hexagon-island density d is defined as n/L, where n is the average number of islands calculated at a given growth time t at the CNT end-rim, and L denotes the system circumference or the number of vertices needed in the CNT edge mapping. Since L is a constant for the system, d behaves and will be considered as n. The average island size l is defined as the average total number of hexagons in all islands observed at the CNT edge divided by the average number of islands (see Figure 5).

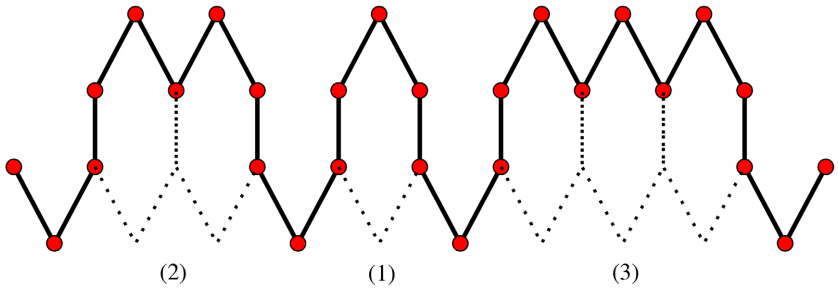

Figure 5. (color online) Schematic representation of a portion of a growing CNT rim with three hexagon-islands with an average island size of value $l=2$.

4. Results and Discussion

Before displaying our results, it is worth noting that, in surface growth processes, when the diffusion length Γ increases, the diffusion ability of landed atoms increases. These atoms can then move a longer distance before being incorporated in a step/island, or meeting other diffusing adatoms to make an irreversible aggregation. This, of course, strongly affects the islands statistics.

In Figure 6, we illustrated the average island size l (panel (a)) and the island density d (panel (b)) as functions of the growth time $t=N/F$ at selected values of the diffusion length Γ for a CNT with zero chirality. The simulation temperature is fixed to $T=10$. At this value, we think that most deposition and diffusion kinks may be activated. All reported results have been averaged over 10^4 independent runs in view to get smooth simulation data. At very small CNT rim coverages, an increase in both l and d is observed. This physically indicates that small hexagon-islands are formed at the CNT rim. They grow over time by receiving either adsorbing or diffusing carbon atoms at their edges to get larger and larger. It is noteworthy that after a certain growth period, l and d pass by a maximum, after which they decrease. When d decreases and l increases, this means that growing hexagon-islands are merging, coalescing. This process may lead in appropriate growth conditions to the formation of a complete atomic layer on the CNT edge before island nucleation occurs above. For $\Gamma=1$, this event approximately occurs in the time interval $N=45-63$. In that case, at low carbon atom mobility (low Γ), the formation of several growing atomic layers may occur and complex behaviors of l and d may result. Let us remark that for $\Gamma=1000$, values of l and d are lower than those obtained for other values of

Γ. Comparing the calculated values of these quantities and the number of carbon atoms deposited, one may conclude that atom diffusion mainly leads to the formation of open hexagons *i.e.*, to the proliferation of correlated vertices of type 4 at the CNT rim. The reduction of atom migration lowers the apparition of these vertices and enhances d and l, at least in the submonolayer regime ($N \le L$). Also, lowering the temperature should have the same effect by activating closing of open hexagons and thus the increase of d and l.

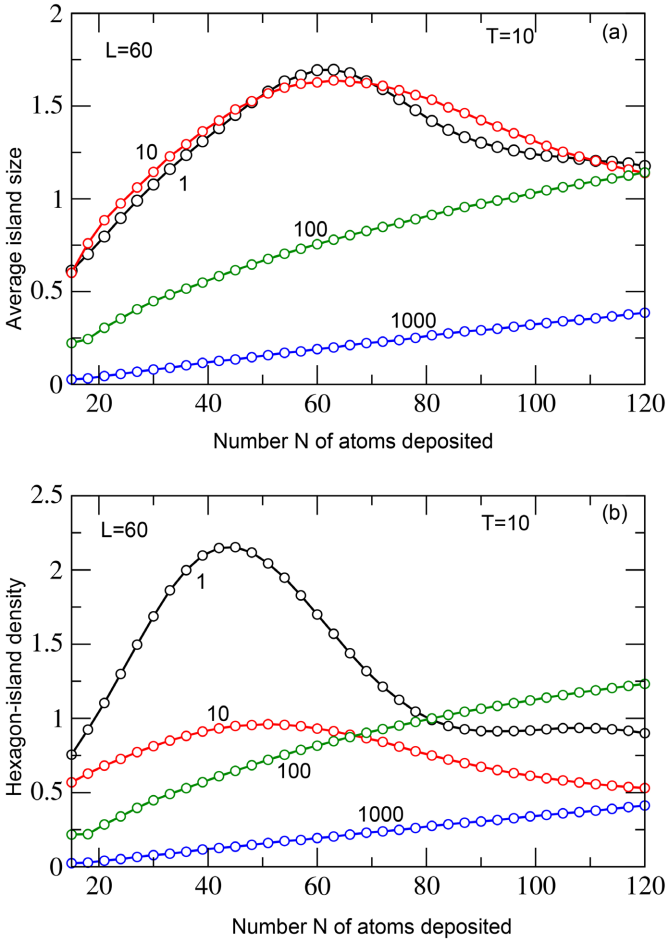

Figure 6. (color online) Average hexagon-island size l (a) and hexagon-island density d (b) as functions of the number $N = F \times t$ of deposited carbon atoms on the CNT rim at the temperature $T = 10$ for a few values of the diffusion length Γ written on the curves. A CNT system with length $L = 60$ and zero chirality is the one investigated.

In **Figure 7**, the behaviors of 2-hexagon (panel (a)), 4-hexagon (panel (b)) and 6-hexagon islands' densities for selected values of Γ are illustrated as functions of the number N of deposited carbon atoms. We used in the calculations $L = 60$, $T = 10$ and $c = 0$. It could be observed from different panels that the islands density shows a decreasing trend with the island size. This means that the probability to find a large island with six hexagons at the CNT rim is rather weak.

Moreover, the density in each panel increases with the growth time N, then shows a maximum after which it decreases. The increasing part has an exponential trend, and the growth time $t_{\max}$ needed to reach the maximum does not change too much for $\Gamma = 1$ and $\Gamma = 10$, whereas for $\Gamma = 100$ and $\Gamma = 1000$, it sharply increases. Comparing **Figure 6(b)** with **Figure 7(a)**, one can conclude that most hexagon-islands are of sizes 1 or 2. Let us remark that for $\Gamma = 1,10$ the early growth time behavior of the island density in all panels, bears some resemblance with a Gaussian shape. The deviation from this behavior becomes important for large values of Γ at high CNT rim coverages.

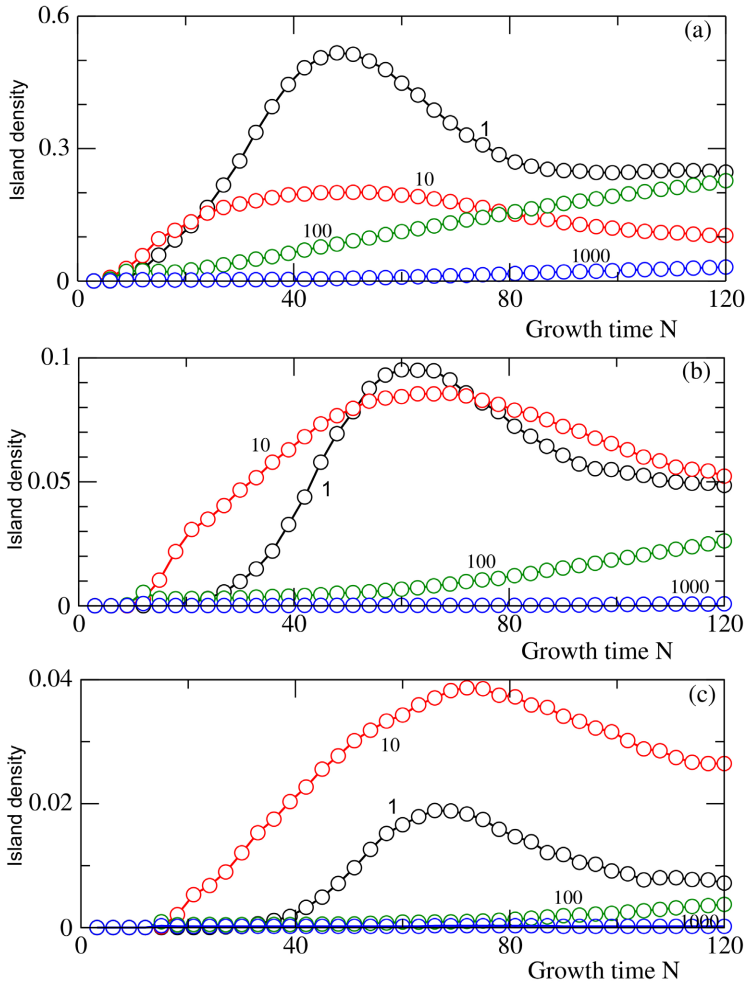

Figure 7. (color online) Densities of islands with two (a), four (b), six (c) hexagons at temperature $T = 10$ as functions of the growth time N. Four selected values of the diffusion length Γ written on the curves are considered. A CNT rim with length $L = 60$ and zero chirality ($c = 0$) is considered.

In **Figure 8**, we displayed the behaviors of the islands density d and the average islands size l for a CNT of chirality $c = 4$ at three values of Γ, at $T = 10$. The initial sample has four equidistant dislocation steps. A global maximum is observed for each curve in both panels. By comparing **Figure 8** and **Figure 6**, one

can get some insight into the effect of chirality during SWCNT growth. First, it emerges that the presence of chirality lowers both l and d, in particular at high coverages. This is physically acceptable due to diffusion of carbon atoms to preexisting dislocation steps, which are absent on zigzag CNT. Second, one remarks that l and d continuously vanish after about three hexagon monolayers have been deposited. This feature may have two origins. Either fast diffusion to steps depletes landing atoms from terraces located between dislocation steps, which mechanism may normally induce step-flow growth mode on the CNT, or the CNT rim roughens with several hexagon layers growing at the same time. Another origin may be the advent of growth instability, with the appearance of large local slopes at the CNT rim with almost no place for islands nucleation. At $\Gamma = 100$, diffusion processes becomes more important and one observes some oscillations in d and l. This feature may be associated to hexagon-islands nucleation and coalescence events at the CNT rim.

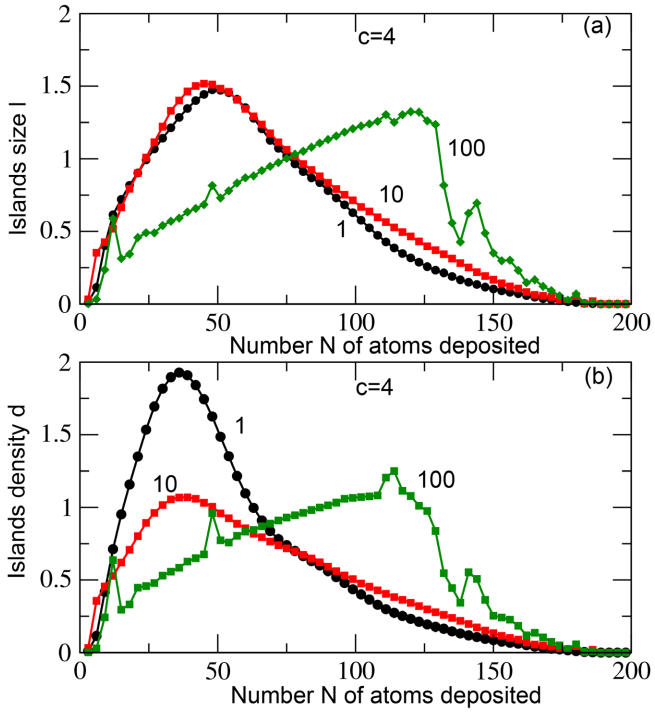

Figure 8. (color online) Simulated average islands size l (panel (a)) and average islands density d (panel (b)) for a chiral CNT characterized by $L = 60$ and $c = 4$ at three values of the diffusion length Γ written on the curves. The simulation temperature is fixed to $T = 10$. The figure gives an insight into the effect of chirality on both d and l in comparison with results from Fig.6 where data concern a CNT with zero chirality.

In **Figure 9**, the effect of the CNT chirality on 1-hexagon islands density is illustrated for two values of the parameter Γ. In panel (a), it could be observed that beyond the early time growth, the island density decreases with increasing values of the chirality parameter c. Moreover, the growth time associated with the maximum density shifts to lower values with the increase of c. Another remark is

that when c increases, the Gaussian shape of the 1-hexagon islands density becomes more and more pronounced. In our opinion, these observations make some physical sense. Indeed, at the beginning of the growth process, there are numerous adsorption sites and the total growth rate of initial configurations exceeds that of the migration sites. Carbon atoms deposition on terraces may occur and lesser diffusion processes may follow. This enhances 1-hexagon islands formation and justifies the early-time increase of the density in both panels. This situation will be reversed during the growth depending on how important is the value of Γ. Thus, landed carbon atoms will migrate to steps and be incorporated there. This situation will minor 1-hexagon islands formation on terraces. Higher is the steps density or the value of the CNT chirality c, lower should be the density of the island measured on terraces.

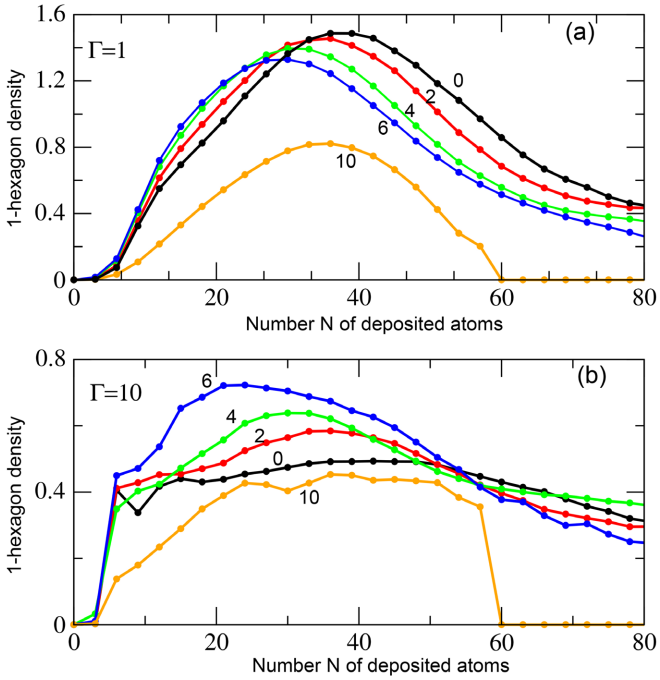

Figure 9. (color online) Densities of 1-hexagon island for $\Gamma = 1$ (panel (a)) and $\Gamma = 10$ (panel (b)) at selected values of the nanotube chirality c written on the curves in each panel. The value $c = 2$ for example, indicates that the growing CNT rim has initially an axial dislocation with two preexisting dislocation steps. In the panels, zigzag and chiral CNTs of size $L = 60$ are considered. At $\Gamma = 1$, an increase of the CNT chirality is followed by a decrease of the density in the stationnary growth regime.

In **Figure 10**, the behavior of the average islands density d is illustrated for CNT rims with different chiralities. It could first be noted that with increasing values of the parameter c, the average island density decreases. This indicates that, with the decrease of the average terrace width between dislocation steps, hexagon-islands formation on terraces becomes unlikely due to fast carbon atom diffusion to dislocation steps. One can then speculate that terrace defects density (or kinetic processes on terraces) are affected by the average terrace width, which in

turn, depends on step-step interactions. Some discussions about terrace width distribution on stepped Ag(110) and Au(110) surfaces could be found in Ref. [32]. From different panels, it emerges that simulated densities (full circles) could be best-fitted to Gaussian functions at least in the early stage of the CNT growth process (full lines). The equation of the Gaussian fitting curves has the usual form of probability density:

$$P(t)=\frac{1}{\sigma\sqrt{2\pi}}\exp\left(-\frac{(t-\mu)^2}{2\sigma^2}\right), \tag{4.1}$$

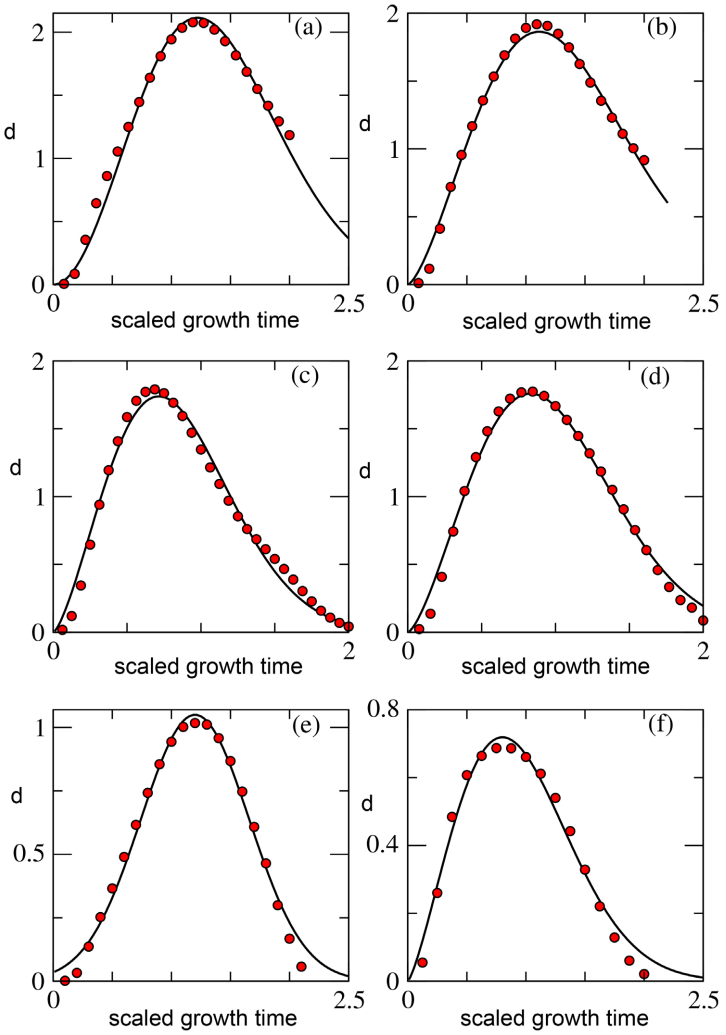

Figure 10. (color online) Averaged hexagon-island densities (full circles) versus scaled growth time calculated on CNT rims with chirality $c=2,4,6,8,10,12$ (panels (a)-(f)) or screw dislocation steps. Values of other parameters used are: $\Gamma=1$, $L=60$, $T=10$. These results have been approximately fitted to a Gaussian behavior (full lines).

where t denotes the scaled growth time. This result, in our sense, agrees with the central limit theorem known in probability theory since the average island density bears some resemblance with the standard normal distribution. The

advent of this trend is not surprising since such probability density is often used to model natural phenomena issued from several random events. We can conclude that the average island density follows a Gaussian behavior with the scaled growth time t in the early stage of the CNT growth process.

In Figure 11, the behaviors of 1- and 2-hexagon islands densities are displayed as functions of the scaled growth time t for selected model parameters: $\Gamma = 1$; $c = 2,4,6,8$ (full circles). It results in the same church bell behavior being observed in all panels for the simulated data. The scaling trend is not trivial. Our analysis best-fitted data to the generalized Wigner distribution (GWD, full lines) whose form reads:

$$P_\rho(t) = a_\rho \times t^\rho \exp\left(-b_\rho t^2\right). \tag{4.2}$$

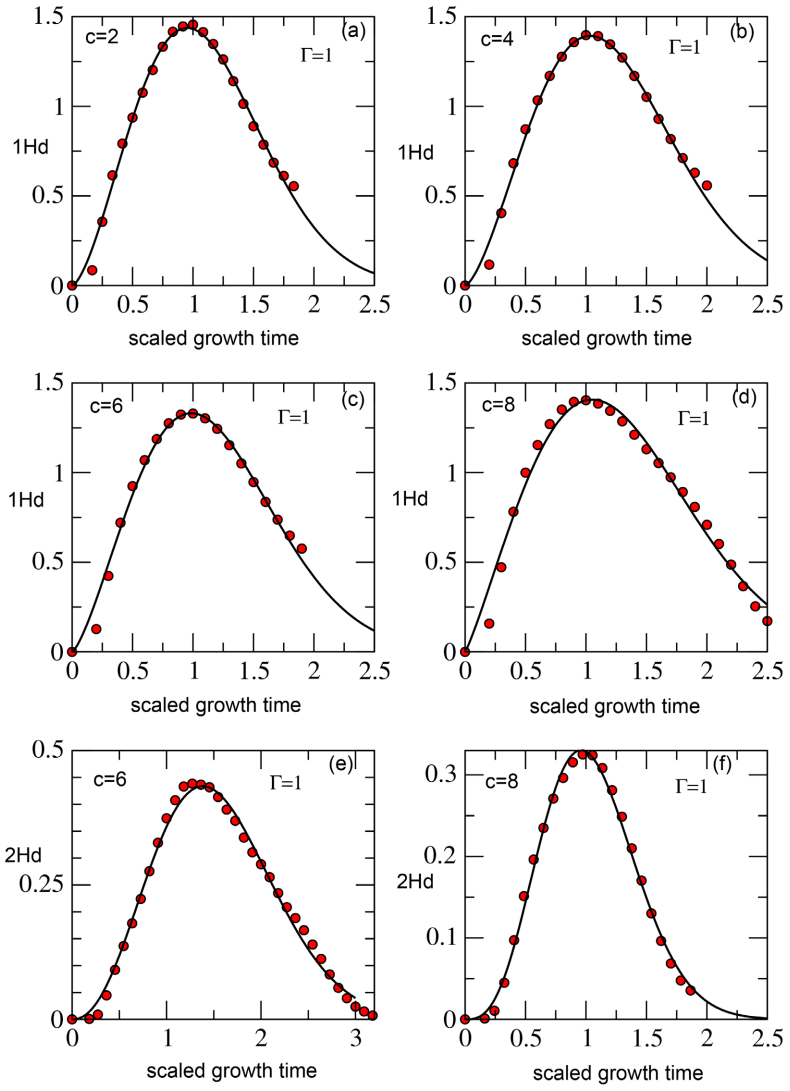

Figure 11. (color online) Simulated 1-hexagon islands density (1Hd) (panels (a)-(d)) and 2-hexagon islands density (2Hd) (panels (e), (f)) versus scaled growth time calculated on CNT rims with chirality $c = 2,4,6,8$. Values of other parameters are: $\Gamma = 1$, $L = 60$, $T = 10$. These results have been approximately fitted to a Generalized Wigner Distribution

(full lines) at the initial stage of the growth process.

where ρ, a_ρ and b_ρ are the distribution parameters. Such a GWD behavior has been obtained in the study of Ag/Ag(110) and Au/Au(110) stepped surfaces for the terrace width distribution (TWD) in ref. [32] in some model parameters' ranges. It has also been observed for vicinal surfaces in the case of steps with alternating stiffness [33]. The step-step interaction potential in this case was taken as repulsive in the form: $V(S)=A/S^2$ where S is the terrace width and A an interaction constant. The effective interaction between steps is believed to be generated by surface relaxation, reconstruction and surface electronic states. It could be remarked that in **Figure 12**, where Γ takes a higher value, the GWD described less well simulated data. How can we explain this behavior? It is obvious that with the axial dislocations, we do have almost equidistant dislocation steps, separated by terraces whose width changes during the growth either by carbon atoms adsorption or by atoms diffusion on terraces. Therefore, the densities of the 1- or 2-hexagon islands obtained after nucleation and growth events and associated TWDs are closely related. It is likely that they show the same trend. This means that in the model, an estimation of the TWD may reveal its GWD behavior since the island's statistics do.

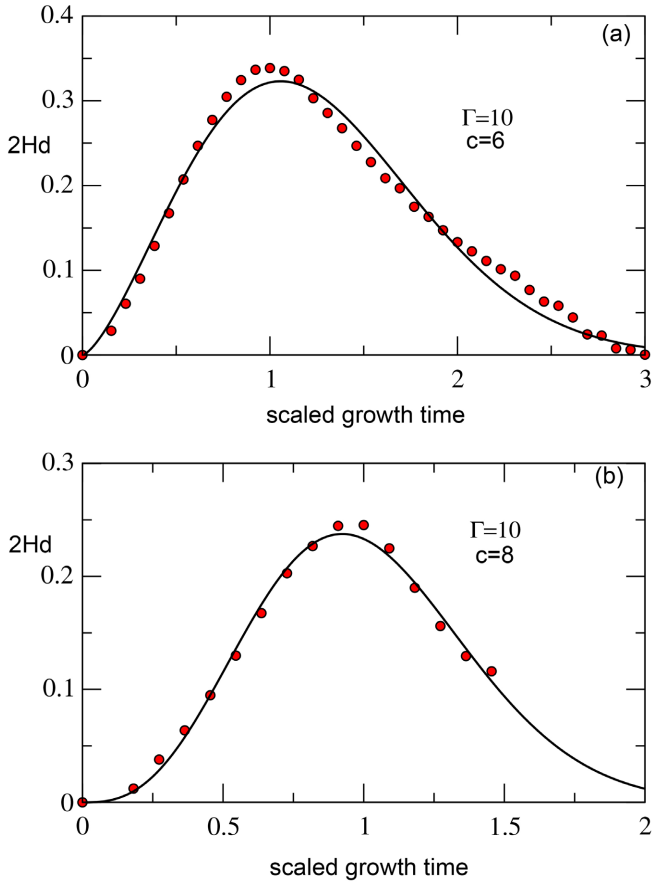

Figure 12. (color online) Simulated 2-hexagon islands density (2Hd) (full circles) versus scaled growth time calculated on CNT rims with chirality $c=6,8$ (panels (a), (b)) for

$\Gamma = 10$. These data have approximately fitted the GWD behavior.

In Figure 13 and Figure 14, the island size distribution is illustrated at different growth times for $\Gamma = 1$. The behaviors are in the form: $p(x) \simeq \exp(-ax)$ since $\log(p)$ behaves linearly with the island size up to $N = 120$. The probability of finding a large island on the CNT rim is extremely weak. It is almost zero for 5- and 6-hexagon islands at low and very high coverages. The 1-hexagon island's density is the most important one at all growth times, being several times higher than that of the 2-hexagon island's density.

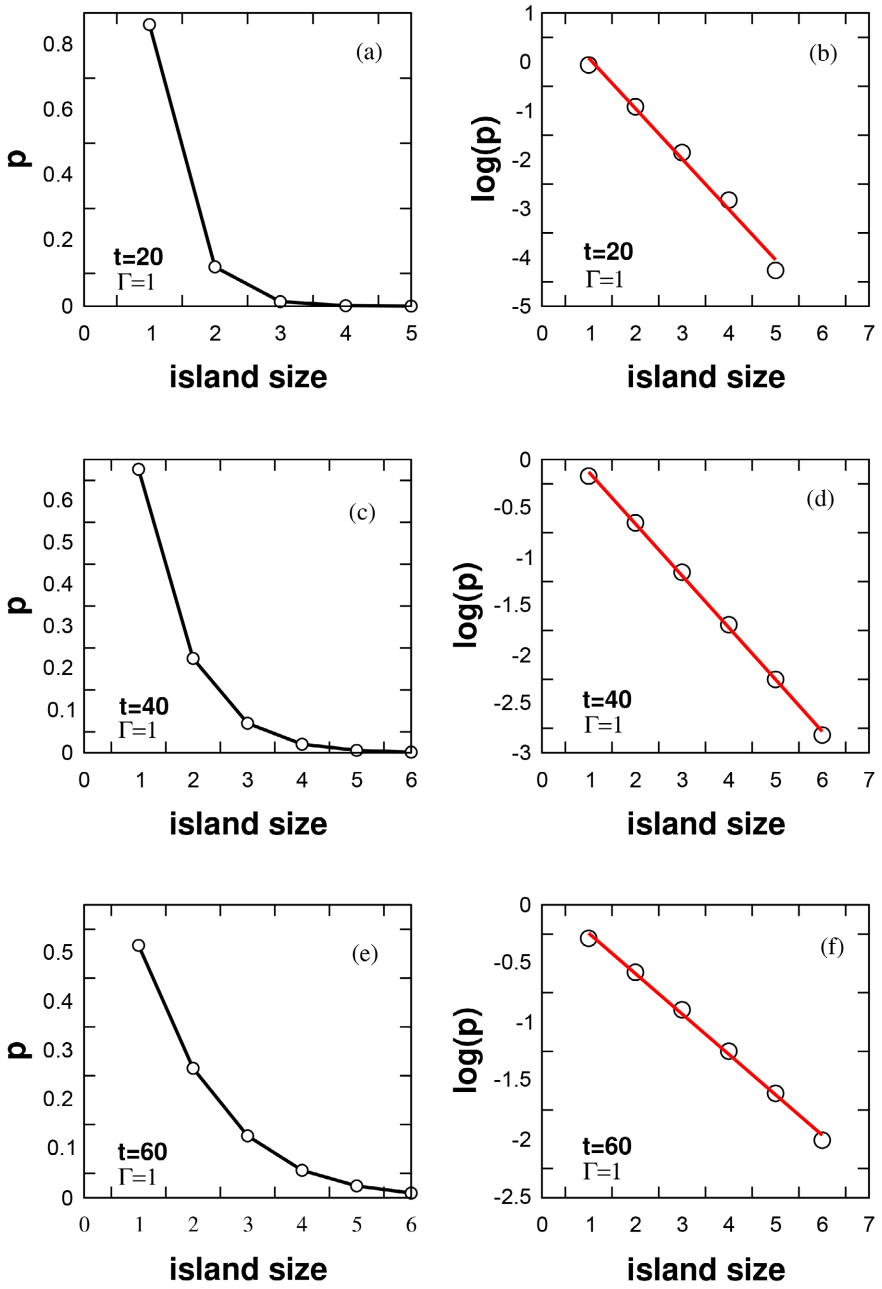

Figure 13. (color online) Simulated data on island size distribution during a zig-zag CNT growth (panels (a), (c), (e)) and corresponding regression curves (panels (b), (d), (f)) at

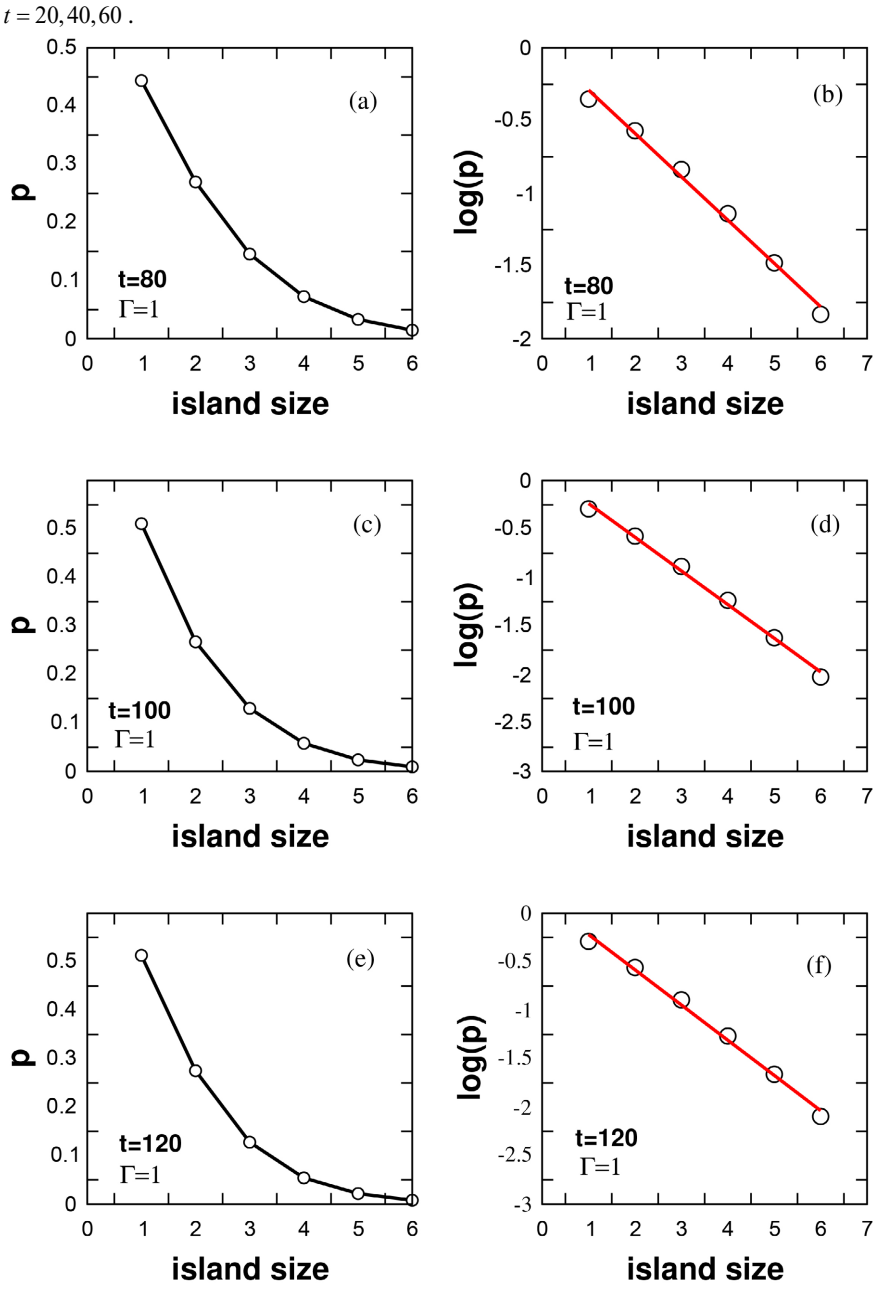

Figure 14. (color online) Simulated data on island size distribution during a zig-zag CNT growth (panels (a), (c), (e)) and corresponding regression curves (panels (b), (d), (f)) at $t = 80,100,120$. It results an exponential decreasing behavior of the island's size distribution with the growth time.

5. Conclusion

As in crystals growth, we studied in this work, islands statistics on growing chiral SWCNTs by means of numerical simulations of a kinetic vertex model. This allowed us to derive the character of new hexagon layers growth on the SWCNT end-rim. The growth occurs by pre-existing steps propagation in some ranges of model parameters. Deviations from this growth mode were apparent at large

deposition rates and small diffusion lengths Γ as well as at high coverages. The SWCNT chirality parameter also affects the growth mode as it can be observed from different islands statistics. Non-trivial behaviors of the islands density with model parameters have been observed. We found that the average islands density displays a Gaussian behavior in the early stage of the growth for appropriate values of model parameters. This trend becomes more accurate when the chirality parameter increases. Beyond that, densities in the 1- and 2-hexagon islands have shown different behaviors. They followed the GWD often obtained for the TWD in stochastic growth models of vicinal surfaces. One can speculate that during the growth, step-step interactions were effective, and TWDs were, of course influenced by hexagon-islands nucleation events on terraces. We also studied the island size distribution at selected growth times for $\Gamma = 1$ and observed that it follows a decreasing exponential behavior. Although the present research work reveals interesting results from the fundamental point of view, it can stimulate many experimental works and be exploited for catalysis as well as for the growth of other nanostructures at steps as it happens for vicinal surfaces in crystals growth.

Author Contributions

All authors equally contribute to the present work in the calculations and in the manuscript writing process.

Conflicts of Interest

The authors declare no conflicts of interest regarding the publication of this paper.

References

[1] Venables, J.A. (2000) Introduction to Surface and Thin Film Processes. Cambridge University Press. https://doi.org/10.1017/cbo9780511755651

[2] Mo, Y.W., Kleiner, J., Webb, M.B. and Lagally, M.G. (1991) Activation Energy for Surface Diffusion of Si on Si (001): A Scanning-Tunneling-Microscopy Study. *Physical Review Letters*, **66**, 1998-2001. https://doi.org/10.1103/physrevlett.66.1998

[3] Ernst, H., Fabre, F. and Lapujoulade, J. (1992) Nucleation and Diffusion of Cu Adatoms on Cu (100): A Helium-Atom-Beam Scattering Study. *Physical Review B*, **46**, 1929-1932. https://doi.org/10.1103/physrevb.46.1929

[4] Amar, J.G. and Family, F. (1996) Characterization of Surface Morphology in Epitaxial Growth. *Surface Science*, **365**, 177-185. https://doi.org/10.1016/0039-6028(96)00692-9

[5] Lobo, L.S. and Carabineiro, S.A.C. (2021) Kinetics of Carbon Nanotubes and Graphene Growth on Iron and Steel: Evidencing the Mechanisms of Carbon Formation. *Nanomaterials*, **11**, Article 143. https://doi.org/10.3390/nano11010143

[6] Bartelt, M.C., Tringides, M.C. and Evans, J.W. (1993) Island-Size Scaling in Surface Deposition Processes. *Physical Review B*, **47**, 13891-13894. https://doi.org/10.1103/physrevb.47.13891

[7] Ferrando, R., Hontinfinde, F. and Levi, A.C. (1997) Morphologies in Anisotropic Cluster Growth: A Monte Carlo Study on Ag (110). *Physical Review B*, **56**, R4406-R4409. https://doi.org/10.1103/physrevb.56.r4406

[8] Hontinfinde, F., Videcoq, A., Montalenti, F. and Ferrando, R. (2004) Leapfrog-Induced Selective Faceting in the Growth of Missing-Row (110) Surfaces. *Chemical Physics Letters*, **398**, 50-55. https://doi.org/10.1016/j.cplett.2004.09.008

[9] Mottet, C., Ferrando, R., Hontinfinde, F. and Levi, A.C. (1998) A Monte Carlo Simulation of Submonolayer Homoepitaxial Growth on Ag (110) and Cu (110). *Surface Science*, **417**, 220-237. https://doi.org/10.1016/s0039-6028(98)00611-6

[10] Bachilo, S.M., Balzano, L., Herrera, J.E., Pompeo, F., Resasco, D.E. and Weisman, R.B. (2003) Narrow (*n*, *m*)-Distribution of Single-Walled Carbon Nanotubes Grown Using a Solid Supported Catalyst. *Journal of the American Chemical Society*, **125**, 11186-11187. https://doi.org/10.1021/ja036622c

[11] Maruyama, S., Miyauchi, Y., Murakami, Y. and Chiashi, S. (2003) Optical Characterization of Single-Walled Carbon Nanotubes Synthesized by Catalytic Decomposition of Alcohol. *New Journal of Physics*, **5**, 149-149. https://doi.org/10.1088/1367-2630/5/1/149

[12] Omrane, B. (2009) Controlled Growth and Assembly of Single-Walled Carbon Nanotubes for Nanoelectronics. Ph.D. Thesis, University of Victoria.

[13] Cançado, L.G., Takai, K., Enoki, T., Endo, M., Kim, Y.A., Mizusaki, H., *et al.* (2006) General Equation for the Determination of the Crystallite Size L_a of Nanographite by Raman Spectroscopy. *Applied Physics Letters*, **88**, Article 163106. https://doi.org/10.1063/1.2196057

[14] Lacerda, R.G., Teh, A.S., Yang, M.H., Teo, K.B.K., Rupesinghe, N.L., Dalal, S.H., *et al.* (2004) Growth of High-Quality Single-Wall Carbon Nanotubes without Amorphous Carbon Formation. *Applied Physics Letters*, **84**, 269-271. https://doi.org/10.1063/1.1639509

[15] Lamouroux, E., Serp, P. and Kalck, P. (2007) Catalytic Routes Towards Single Wall Carbon Nanotubes. *Catalysis Reviews*, **49**, 341-405. https://doi.org/10.1080/01614940701313200

[16] Yu, F., Yang, M., Li, F., Su, C., Ma, B., Yuan, Z., *et al.* (2012) The Growth Mechanism of Single-Walled Carbon Nanotubes with a Controlled Diameter. *Physica E*: *Low-dimensional Systems and Nanostructures*, **44**, 2032-2040. https://doi.org/10.1016/j.physe.2012.06.007

[17] Zhao, J., Guo, Q., Shi, J., Liu, L., Jia, J., Liu, Y., *et al.* (2009) Carbon Nanotube Growth in the Pores of Expanded Graphite by Chemical Vapor Deposition. *Carbon*, **47**, 1747-1751. https://doi.org/10.1016/j.carbon.2009.02.028

[18] Ding, F., Harutyunyan, A.R. and Yakobson, B.I. (2009) Dislocation Theory of Chirality-Controlled Nanotube Growth. *Proceedings of the National Academy of Sciences*, **106**, 2506-2509. https://doi.org/10.1073/pnas.0811946106

[19] Artyukhov, V.I., Penev, E.S. and Yakobson, B.I. (2014) Why Nanotubes Grow Chiral. *Nature Communications*, **5**, Article No. 4892. https://doi.org/10.1038/ncomms5892

[20] He, M., Wang, X., Zhang, S., Jiang, H., Cavalca, F., Cui, H., *et al.* (2019) Growth Kinetics of Single-Walled Carbon Nanotubes with a (*2n*, *n*) Chirality Selection. *Science Advances*, **5**, eaav9668. https://doi.org/10.1126/sciadv.aav9668

[21] Zounmenou, F., Hontinfinde, R.D. and Hontinfinde, F. (2022) Growth Kinetics of a Single-Walled Carbon Nanotube: Exact and Simulation Results. *Physica A*: *Statistical Mechanics and Its Applications*, **594**, Article 127013. https://doi.org/10.1016/j.physa.2022.127013

[22] Oke, T.D., Hontinfinde, S.I.V., Karimou, M., Zounmenou, F. and Hontinfinde, F. (2022) Atomistic Growth Model with Edge Diffusion for Chiral Carbon Nanotubes.

Physica E: *Low-dimensional Systems and Nanostructures*, **142**, Article 115298. https://doi.org/10.1016/j.physe.2022.115298

[23] Hontinfinde, S.I.V., Kple, J., Oke, T.D., Zounmenou, F., Adda, J. and Hontinfinde, F. (2022) Nanofacet-Density Scaling on Zig-Zag Carbon Nanotubes within the Kinetic 5-Vertex Growth Model. *Physica A*: *Statistical Mechanics and Its Applications*, **608**, Article 128278. https://doi.org/10.1016/j.physa.2022.128278

[24] Wang, Y., Zhang, W., Chen, Y., Zeng, X., Huang, J., Wei, H., *et al.* (2023) Mechanism of Carbon Nanotube Growth in Expanded Graphite via Catalytic Pyrolysis Reaction Using Carbores P as a Carbon Source. *Frontiers in Chemistry*, **11**, Article 1260099. https://doi.org/10.3389/fchem.2023.1260099

[25] Moors, M., Amara, H., Visart de Bocarmé, T., Bichara, C., Ducastelle, F., Kruse, N., *et al.* (2009) Early Stages in the Nucleation Process of Carbon Nanotubes. *ACS Nano*, **3**, 511-516. https://doi.org/10.1021/nn800769w

[26] Ohta, Y., Okamoto, Y., Irle, S. and Morokuma, K. (2008) Rapid Growth of a Single-Walled Carbon Nanotube on an Iron Cluster: Density-Functional Tight-Binding Molecular Dynamics Simulations. *ACS Nano*, **2**, 1437-1444. https://doi.org/10.1021/nn8001906

[27] Jin, C., Suenaga, K. and Iijima, S. (2008) How Does a Carbon Nanotube Grow? An *in situ* Investigation on the Cap Evolution. *ACS Nano*, **2**, 1275-1279. https://doi.org/10.1021/nn800121v

[28] Liu, Y., Dobrinsky, A. and Yakobson, B.I. (2010) Graphene Edge from Armchair to Zigzag: The Origins of Nanotube Chirality? *Physical Review Letters*, **105**, Article 235502. https://doi.org/10.1103/physrevlett.105.235502

[29] Hontinfinde, F. and Touzani, M. (1995) Growth Kinetics of Bcc Crystal Surfaces. *Surface Science*, **338**, 236-246. https://doi.org/10.1016/0039-6028(95)00545-5

[30] Hontinfinde, F., Krug, J. and Touzani, M. (1997) Growth with Surface Diffusion in *d*=1+1. *Physica A*: *Statistical Mechanics and Its Applications*, **237**, 363-383. https://doi.org/10.1016/s0378-4371(96)00435-9

[31] Bortz, A.B., Kalos, M.H. and Lebowitz, J.L. (1975) A New Algorithm for Monte Carlo Simulation of Ising Spin Systems. *Journal of Computational Physics*, **17**, 10-18. https://doi.org/10.1016/0021-9991(75)90060-1

[32] Hontinfinde, S.I.V., Akpo, A.B. and Hontinfinde, F. (2016) Numerical Investigation of the Submonolayer Growth and Relaxation of Stepped Ag (110) and Au (110) Surfaces. *The European Physical Journal B*, **89**, Article No. 215. https://doi.org/10.1140/epjb/e2016-70233-1

[33] Yancey, J.A., Richards, H.L. and Einstein, T.L. (2005) Terrace Width Distributions for Vicinal Surfaces with Steps of Alternating Stiffness. *Surface Science*, **598**, 78-87. https://doi.org/10.1016/j.susc.2005.08.028